The effect of strong longitudinal magnetic fields on dose deposition from electron and photon beams

Alex F. Bielajew
Institute for National Measurement Standards, National Research Council of Canada, Ottawa, K1A 0R6, Canada

(Received 7 December 1992; accepted for publication 19 March 1993)

The use of strong, uniform, longitudinal magnetic fields for external electron and photon beam irradiation is considered. Using the EGS4 Monte Carlo code modified to account for the presence of magnetic fields, dramatic narrowing of penumbra for photon and electron irradiations is demonstrated. In the vicinity of heterogeneities, "hot" and "cold" spots due to multiple scattering in electron beams are reduced substantially. However, in the presence of strong magnetic fields, the effect of inhomogeneities can be observed far from the location of the inhomogeneity due to reduced "washout" caused by lateral multiple scattering. The enhanced "Bragg peak," proposed or calculated by other authors, is not observed on the central axis of broad beams, owing to lateral equilibrium. It is proven that for broad parallel beams, the central axis depth-dose curve is independent of the strength of the external longitudinal magnetic field, as long as it is uniform. However, strong longitudinal magnetic fields can induce enhancements by redirection of the electron fields coming from point sources. Strong uniform longitudinal magnetic fields provide a way of controlling the spreading of electron beams due to multiple scattering, making the electron beams more "geometrical" in character, simplifying dose-deposition patterns, possibly allowing electron beams to be used in new ways for radiotherapy. Photon therapy also benefits from strong uniform longitudinal magnetic fields since the penumbra or other lateral disequilibrium effects associated with lateral electron transport can be eliminated.

Key words: electron, magnetic fields, Monte Carlo, penumbra, radiotherapy

I. INTRODUCTION

External magnetic fields have been considered by several researchers as a means of enhancing dose-deposition characteristics from external electron beams. Bostick[1] proposed the use of longitudinal fields to enhance the "Bragg peak" and performed simple pencil-beam calculations. Weinhous, Nath, and Schulz[2] performed Monte Carlo calculations interpreting their results to be in agreement with Bostick's model. As well, Weinhous *et al.* executed a design study, demonstrating that a compact, single-coil superconducting magnet producing a 6-T field in its 20-cm core could be manufactured. One study by Sempert[3] advocated the use of magnetic fields external to the patient, which causes the electron beam to converge at the tumor site. Following Shih's Monte Carlo study of lateral fields to deflect electron beams towards tumor sites within the patient,[4] several experimental studies using lateral fields have been published for homogeneous[5–7] and heterogeneous[8] phantoms.

The current study is motivated for several reasons.

(1) Stronger magnetic fields may be produced more cheaply if manufacturing techniques are able to make use of high-T_c superconducting materials.

(2) There have been advances in calculational techniques. A recent theoretical study[9] demonstrated that the effect of external magnetic fields of an arbitrary configuration can be calculated with high accuracy in a condensed-history electron Monte Carlo code.

(3) The interpretation of Weinhous *et al.*[2] that the enhancement on the central axis of point source electron beams in uniform fields is a Bragg peak is erroneous. It will be demonstrated later that this effect is the result of the magnetic fields straightening the point source skewness of the electron beam producing a fluence enhancement along the central axis.

(4) The effect on electron transport near heterogeneities in the presence of longitudinal fields has not yet been investigated.

(5) The effect of longitudinal fields on the penumbra of electron and photon beams has yet to be investigated.

The Monte Carlo calculations in this study were performed using the EGS4 code system[10] modified to account for external magnetic fields[9] and incorporating the accurate electron transport algorithm, PRESTA.[11] The collision and radiative stopping powers employed were the same as specified in ICRU Report No. 37.[12–14] The EGS4 user code, DOSRZ, a cylindrical-planar dose-scoring code, has been used in other studies for benchmarking purposes at low energy (^{60}Co energy)[15] and high energy (10 and 20 MeV).[16]

The capability for transport in external fields is implemented via a "macro package," which is independent of the user code. When included at the compilation stage, neither the EGS4 system nor user code require modification. (This macro package is available from the author on request.)

 0094-2405/93/20(4)/1171/9/$1.20

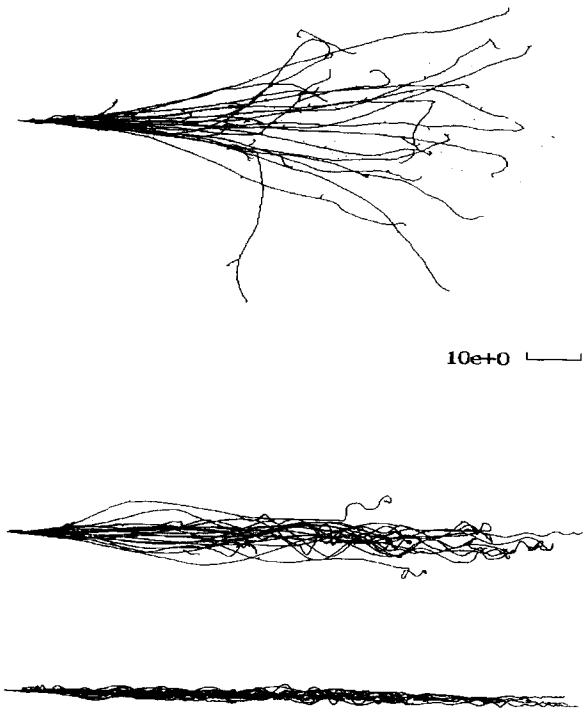

FIG. 1. Twenty histories of 20-MeV electrons are transported through water in the presence of uniform, longitudinal magnetic fields. Top: 0 T, middle; 6 T; bottom: 20 T. The range of 20-MeV electrons in water is about 9.3 cm, and this is the longitudinal extent of the trajectories depicted. A 1-cm scale marker is also shown.

II. ELECTRON BEAMS

A. General features

1. Radial confinement

While in vacuum in the presence of uniform magnetic fields, electrons are known to spiral about magnetic field lines in a helical orbit with a gyration radius, r_g, given by

$$r_g=\frac{p_\perp}{3.00B}, \tag{1}$$

where r_g is measured in cm, $p_\perp$, the momentum of the electron perpendicular to the direction of the magnetic field, measured in MeV/c, c is the speed of light, and B is the magnetic field strength measured in Tesla (T).[17]

In media, the helical structure is still present, but the regularity of the helical paths is broken by the stochastic nature of elastic Coulomb scattering, knock-on, and bremsstrahlung processes. Generally, small energy losses cause the gyration radius to shrink while a large angle component of Coulomb scattering can cause large increments or decrements in $p_\perp$, making the helicity appear to change discontinuously. These features are depicted in Fig. 1, where a 20-MeV pencil beam in water is subject to a longitudinal field of 0, 6, and 20 T. These simulations represent 20 incident particle histories for each magnetic field strength. (These pictures were produced using a graphical interface to the EGS4 system.)[18] Photon transport was "switched off," although the energy straggling associated with bremsstrahlung production was modeled. Electrons were tracked until their kinetic energy fell below 189 keV.

The gyration radii for these examples are 1.11 cm (for 6 T) and 0.33 cm (for 20 T). Most of the primary transport takes place within the envelope of the gyration radius, although scattering events can force electron tracks outside. (One can imagine an extremely rare event where multiple scattering exactly undoes the bending due to the external magnetic field!) This general behavior is exhibited by the tracks in Fig. 1. Energy deposition far outside the gyration radius can occur through second-order processes intermediated by photons (e.g., electrons set in motion by bremsstrahlung photons). Evidence of this behavior will be seen in the more quantitative discussion following.

A "rule of thumb" may be devised to determine a threshold below which longitudinal magnetic fields would have no effect on electron transport. This may be done by equating the gyration radius of Eq. (1) to a crude estimate for the range, r_0, of an electron, $r_0=\rho E/2$, where ρ is the material density and E is the kinetic energy in MeV. This "rule of thumb" for the threshold longitudinal field is $B(\mathrm{T})>2\rho(\mathrm{g/cm^{-3}})/3$ and only applies in the relativistic regime, $E\gg 0.511$ MeV. More sophisticated estimates may be derived for the nonrelativistic regime or more accurate energy-range relationships used,[19] but for our purposes, $B(T)>\frac{2}{3}$ for water suffices.

In the remainder of this study, only 3 and 20 T uniform longitudinal fields within the phantom are considered. The lower value is representative of field strengths obtainable easily in the laboratory or hospital, while the higher value is representative of the limits of the modern magnet design. The effects of fringing fields outside the phantom are not considered in this report. These effects have been considered by Weinhous *et al.*[2]

2. Additional synchrotron radiation

While in the presence of an external magnetic field, synchrotron radiation is generated by virtue of the bending of the electron trajectories.[17] To place an upper estimate on this effect, the power radiated as synchrotron radiation for an electron undergoing a purely circular orbit is[17]

$$P=\frac{2}{3}\frac{e^2c}{r_g^2}(\gamma^2-1)^2, \tag{2}$$

where e is the charge of the electron, c is the speed of light, β is the speed of the electron divided by the speed of light, and γ is the relativistic factor $(1-\beta^2)^{-1/2}$.

In the relativistic limit ($\beta\to 1$), the additional stopping power attributable to synchrotron radiation, dE_s/dx, is

$$\frac{dE_s}{dx}=\lim_{\beta\to 1}\frac{P}{\beta c}=1.27\times 10^{-5}E^2B^2, \tag{3}$$

where E is the total energy in MeV and B is the field strength in T, and dE_s/dx is measured in eV/cm.

For a 50-MeV electron beam in a 20-T field undergoing a purely circular orbit, this additional stopping power amounts to about 13 eV/cm. Hence, for radiotherapy where energy dissipation occurs in the MeV/cm range,

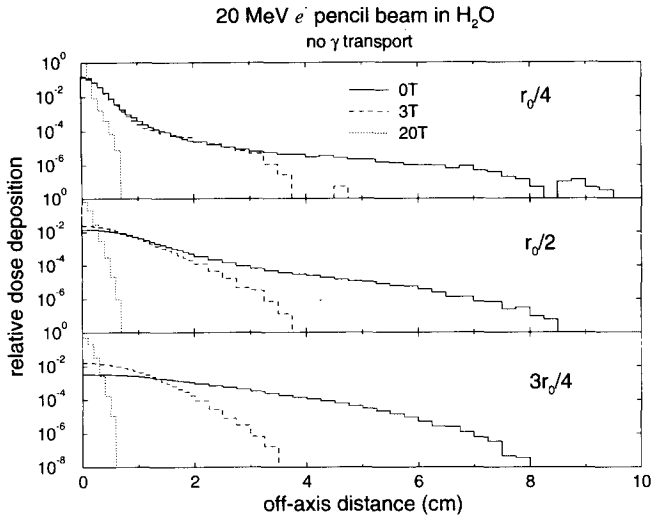

FIG. 2. 100 000 histories of 20-MeV electrons are transported through water in the presence of uniform, longitudinal magnetic fields with strengths 0, 3, and 20 T. Radial profiles are shown at depths of $r_0/4$, $r_0/2$, and $3r_0/4$. In this case, any photons set in motion through bremsstrahlung or pair annihilation were absorbed on the spot. The 3-T histograms are depicted by dashed lines.

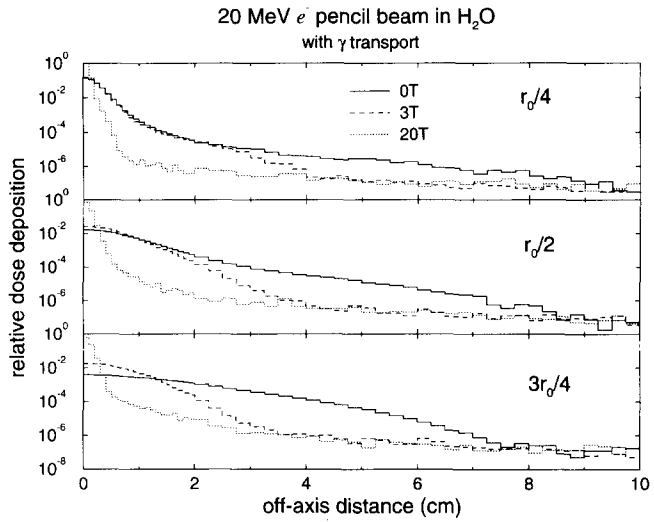

FIG. 3. The same simulations as in Fig. 2, but with photon transport above 10 keV turned on. When a photon fell to 10 keV, its energy was absorbed on the spot.

radiative losses due to synchrotron radiation for electrons in external magnetic fields can be ignored, both in terms of the additional slowing down of the electrons and the energy deposition at remote locations due to the transport of the synchrotron photons.

B. Pencil beams

To investigate the effects of magnetic fields on pencil beams, 100 000 electrons were simulated with monoenergetic incident energy of 20 MeV incident on a water phantom $5r_0/4$ in depth (r_0 is the range, which is 9.32 cm at 20 MeV)[12] and 10 cm in radius. Electron transport was effected until the electron energy fell to 189 keV, at which point the residual energy was deposited on the spot. The data represented in Fig. 2 show radial profiles at depths of $r_0/4$, $r_0/2$, and $3r_0/4$ for longitudinal magnetic fields of 0, 3, and 20 T. In this case, any photons created by bremsstrahlung or pair annihilation processes were absorbed on the spot to isolate the effect on electron transport. The 8% radiative yield[12] is therefore included in the energy deposition. The data are normalized to the 20-T central axis datum at the depth of $r_0/4$. Most of the electron transport takes place within the gyration radii (2.2 cm for 3 T, 0.33 cm for 20 T), save for some leakage due to the stochastic processes at the level of 10^{-4}–10^{-3}. One notes the strong confinement of the beam within the gyration radii and decreasing outscatter along the central axis as the longitudinal field strength increases.

The same set of simulations were performed with photon transport switched on. (Photons were transported until their energy fell to 10 keV, at which point the energy was deposited on the spot.) The data are shown in Fig. 3. Independent of the external magnetic field strength, the energy deposition converges to the same value (within statistics) of about 10^{-7} far outside the gyration radii. There is no narrowing of the bremsstrahlung component. Although the magnetic field changes the azimuthal direction of the electrons, it does not change its magnitude. Since the scoring shells in the cylindrical-planar geometry are azimuthally symmetric and the magnetic field preserves the azimuthal symmetry, one expects the same relative bremsstrahlung contribution. There should be an absolute difference associated with increased photon attenuation. The higher the magnetic field strengths, the closer to the central axis the photons are released. Thus, to reach the same outer radius the photons produced in the presence of magnetic fields undergo more attenuation. However, within the precision of the calculation, this effect was not observed. This is not unexpected, in view of the fact that the photon mean-free path ranges from 14 cm for 1-MeV photons in water to 55 cm for 20 MeV.

C. Central axis dose deposition for broad parallel beams

To study the effect of longitudinal magnetic fields on the central axis of broad parallel beams, simulations were performed for 20-MeV electrons on water phantoms. The phantom depth was chosen to be $5r_0/4$ as before, but the phantom width was effectively infinite (1000 cm was actually used). [Rather than scoring the dose deposition on the central axis due to a broad beam, the beam employed was a pencil beam and the dose in the entire phantom was scored as a function of depth. The answers are equivalent and may be derived in complete generality by a symmetry argument (the Geometry-Equivalence Theorem).[20] However, the computational efficiency is dramatically enhanced.]

The results for 100 000 incident electrons from a broad, parallel beam with magnetic field strengths of 0, 3, and 20 T are shown in Fig. 4. One notes that the three histograms are virtually identical. There is no evidence of a "Bragg

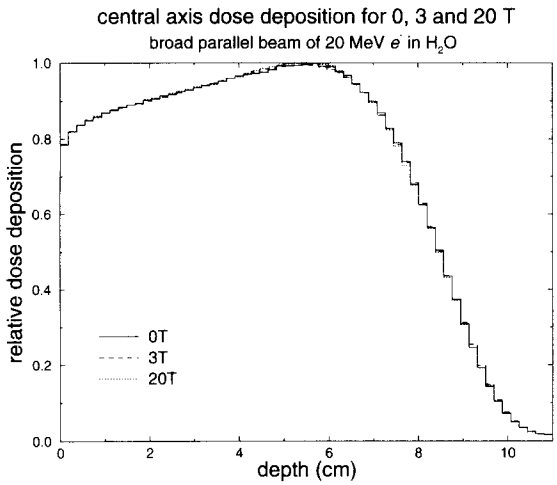

FIG. 4. 100 000 histories of 20-MeV broad, parallel beam electrons are transported through water in the presence of uniform, longitudinal magnetic fields with strengths 0, 3, and 20 T. The central axis depth doses depicted are virtually identical.

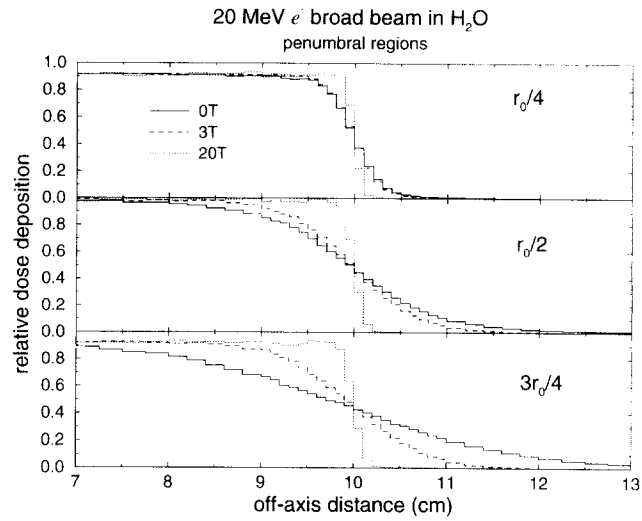

FIG. 5. The 20-MeV electrons are transported through water in the presence of uniform, longitudinal magnetic fields with strengths 0, 3, and 20 T. Penumbral profiles are shown at depths of $r_0/4$, $r_0/2$, and $3r_0/4$.

peak," as suggested by Weinhous *et al.*[2] Bostick's analytical calculations[1] also suggested the appearance of a Bragg peak. However, Bostick's enhancement arose entirely from the increase in average deflection angle and stopping power of an electron as it reaches the end of its range. Since Bostick's model did not include particle loss, range straggling, or lateral transport, his peak is an artifact of the simplicity of his model and applies more to pencil beams rather than broad beams. The peak calculated by the method of Weinhous *et al.* is due to fluence enhancement, as a result of the electrons' point source distribution being straightened by the uniform magnetic field. This point is elaborated upon in the next section.

That the central axis depth dose curves in broad parallel beams should be independent of longitudinal field strength follows from the condition of lateral equilibrium. In a broad beam along the central axis where full lateral equilibrium is established, the lack of in-scattering from laterally distant tracks is exactly compensated for by the increased fluence from local tracks.

To make the argument more rigorous, consider a broad parallel beam entering a semi-infinite homogeneous medium. There are no radial boundaries, therefore, any rotation about the longitudinal direction (the normal to the entrance plane of the medium) does not affect the physics or the energy deposition. An electron subject to a longitudinal magnetic field is rotated about the longitudinal axis in the azimuthal direction. Since the medium is azimuthally symmetric and the rotations are not associated with any other physical effects (magnetic fields do not change the energy of a charged particle), there can be no change in energy deposition. A more mathematical development is presented in the Appendix.

D. Penumbra for parallel beams

Penumbral confinement of electron beams is shown in Fig. 5, where 20-MeV electrons were transported through a water phantom with no magnetic field as well as 3- and 20-T uniform fields. The penumbral profiles at depths of $r_0/4$, $r_0/2$, and $3r_0/4$ are shown. While the moderate 3-T field shows little improvement except at $3r_0/4$, the strong 20 T field confines the edge of the beam to within a few millimeters. These data were normalized globally to the maximum of the 0-T data.

E. Point-source effects

The broad parallel beam results call into question the Bragg peak conclusion of Weinhous *et al.* In one of their calculations, they employed a uniform 3-T field within a water phantom irradiated by 20-MeV electrons emanating from a point source 105 cm from the front surface of the phantom with a surface field diameter of 10 cm. Consulting Fig. 2, one sees that the central axis of this configuration is not fully equilibrated. The point-source nature of the incident electron beam also upsets the symmetry arguments given above and in the Appendix. Therefore, this calculation was repeated and the central axis results are given in Fig. 6. These data indicate agreement with the calculations of Weinhous *et al.* Another calculation with a 20-cm field size was done with almost identical results eliminating the possibility that the enhancement was due to incomplete lateral equilibrium. One is forced to conclude that the point source skewness of the incident electron beam is being straightened by the magnetic field. This skewness is "curled up" along the direction of the magnetic field lines, causing an increase in electron fluence. The statement of Weinhous *et al.*, "the magnetic field confined the dose delivered by the electrons to within the geometrical edges of the beam" is accurate only for uniform beams. For point-source beams the magnetic field confines the dose delivered by the electrons to within the cylindrical tube defined by its axis lying along the direction of the magnetic field and its diameter defined by the beam diameter on the phantom surface.

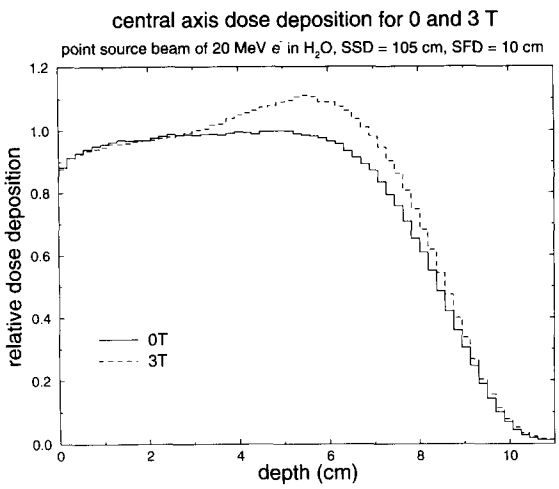

FIG. 6. Central-axis dose distributions from 20-MeV electrons emanating from a point source at 105 cm from the surface of a cylindrical phantom with a field size of 10 cm on the phantom surface with no magnetic field and a 3-T uniform magnetic field within the phantom.

Despite a source to phantom distance of 105 cm, an enhancement of about 10% is observed. This suggests the possibility that SSD's can be manipulated to produce a desired enhancement while confining the beam to treatment regions. To demonstrate this, the point source calculation described above was repeated for SSD's of 20, 50, and 200 cm, with the results plotted in Fig. 7. The 20-cm SSD calculation shows a 20% enhancement over the surface dose, where the zero-field dose is maximum. For 50 cm the enhancement is 15%, 10% for 105 cm, as discussed above, and 5% for 200 cm. Thus for practical treatment distances, enhancements from 5%–15% can be observed.

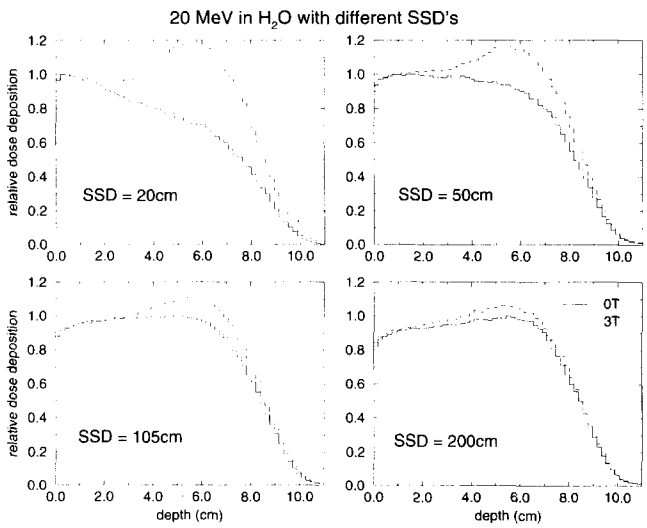

FIG. 7. Central-axis dose distributions from 20-MeV electrons emanating from a point source at 20, 50, 105, and 200 cm from the surface of a cylindrical phantom with a field size of 10 cm on the phantom surface with no magnetic field and a 3-T uniform magnetic field within the phantom.

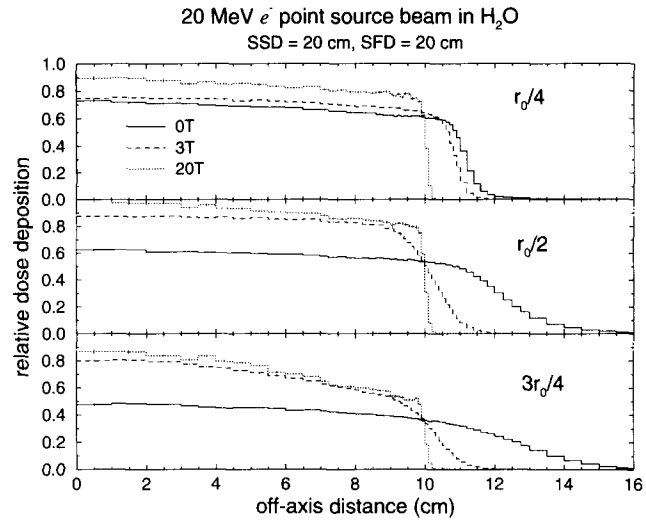

FIG. 8. The 10^6 histories of 20-MeV electrons are transported through water in the presence of uniform, longitudinal magnetic fields with strengths 0, 3, and 20 T. Radial profiles are shown at depths of $r_0/4$, $r_0/2$, and $3r_0/4$. The point source was located 20 cm from the phantom surface collimated to a radius of 10 cm.

The magnetic field also constrains the point-source spreading of the electron beam within the phantom. Figure 8 represents radial profiles at depths of $r_0/4$, $r_0/2$, and $3r_0/4$ for longitudinal magnetic fields of 0, 3, and 20 T for a point source was located 20 cm from the phantom surface collimated to a radius of 10 cm. One may note that the magnetic field attempts to confine the beam to the cylindrical tube lying along the direction of the magnetic field and its diameter defined by the beam diameter on the phantom surface. Thus the point-source spreading of the beam within the phantom is constrained by the external field. However, the $1/r^2$ effect is still evident for the $r_0/4$ and $r_0/2$ profiles, where it is expected that the beam edge to central axis dose ratio should be 0.8 for this example. At the greatest depth depicted, this ratio is smaller, as differential particle attenuation begins to manifest itself. The particles on the beam edge at this depth have traveled farther, their paths being more curved than those near the central axis.

F. Heterogeneities

Since magnetic fields confine electron beams and it is known that scattering from heterogeneities produces strong perturbative effects on electron beam dose distributions,[16,21] magnetic fields can be expected to reduce these perturbations, resulting in more predictable behavior. To this end, Monte Carlo calculations done previously[16] were repeated, but with 3- and 20-T longitudinal magnetic fields and parallel electron beams. The case of a 2-cm long, 1 cm diam air inhomogeneity placed at 2-mm depth in a water phantom and irradiated with a 20-MeV broad parallel beam was investigated. The central axis results are shown in Fig. 9. While the 0- and 3-T results are similar qualitatively, the 20-T field eliminates the perturbation along the central axis, except for a 2-cm range shift of the

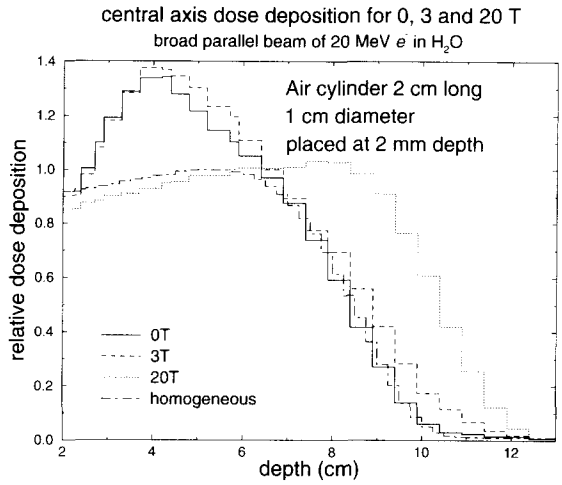

FIG. 9. The 20-MeV electrons are transported through water in the presence of uniform, longitudinal magnetic fields with strengths 0, 3, and 20 T. A 2-cm long, 1-cm diam air inhomogeneity is placed at a depth of 2 mm in the phantom. Central axis dose deposition (in a 5-mm diam scoring region) is depicted. Comparison with the homogeneous calculation is also given.

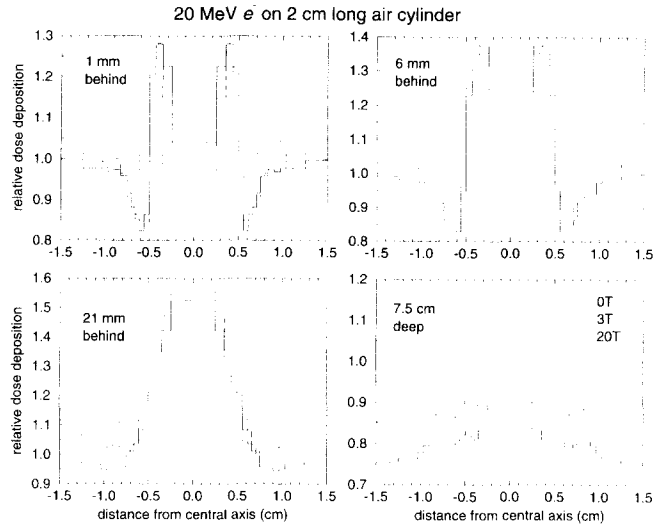

FIG. 11. The 20-MeV electrons are transported through water in the presence of uniform, longitudinal magnetic fields with strengths 0, 3, and 20 T. A 2-cm long, 1-cm diam air inhomogeneity is placed at a depth of 2 mm in the phantom. Radial profiles of dose deposition are depicted 1, 6, and 21 mm behind the inhomogeneity, as well as at a 7.5-cm absolute depth.

depth-dose curve. This behavior is consistent with the interpretation that the beam that passed through the inhomogeneity has been confined to the region near the central axis. Multiple scattering has obliterated the effect of the inhomogeneity for the 0-T case, and nearly so for the 3-T case. The 1-cm long, 1-cm diam aluminium inhomogeneity depicted in Fig. 10 produced similar results, except that the range shift was in the opposite direction.

Radial profiles for these configurations are shown in Fig. 11 and Fig. 12. The 3-T field reduces the size of the perturbation only marginally, while the 20-T case reduces drastically the height and width of the perturbations. Note that the range shift of the electron beam for the 20-T case is quite apparent at 7.5 cm in depth. If a flat field is required at depth, then it is possible that a bolus at the surface could compensate for the underlying heterogeneity.

III. PHOTON BEAMS

A. Pencil beams

Magnetic confinement can also be employed in photon therapy as a way of controlling the electron portion of the

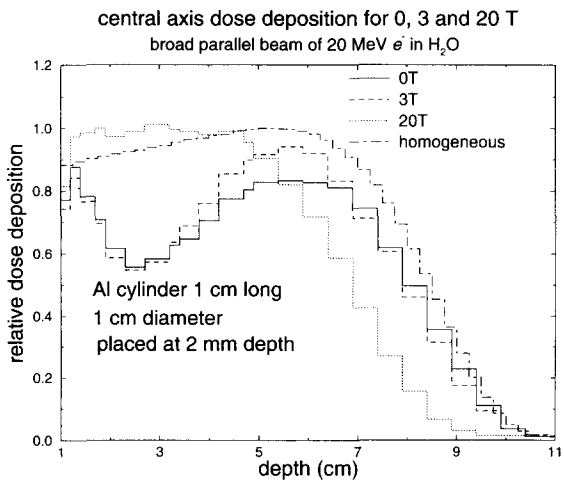

FIG. 10. The 20-MeV electrons are transported through water in the presence of uniform, longitudinal magnetic fields with strengths 0, 3, and 20 T. A 1-cm long, 1-cm diam aluminium inhomogeneity is placed at a depth of 2 mm in the phantom. Central axis dose deposition (in a 5-mm diam scoring region) is depicted. Comparison with the homogeneous calculation is also given.

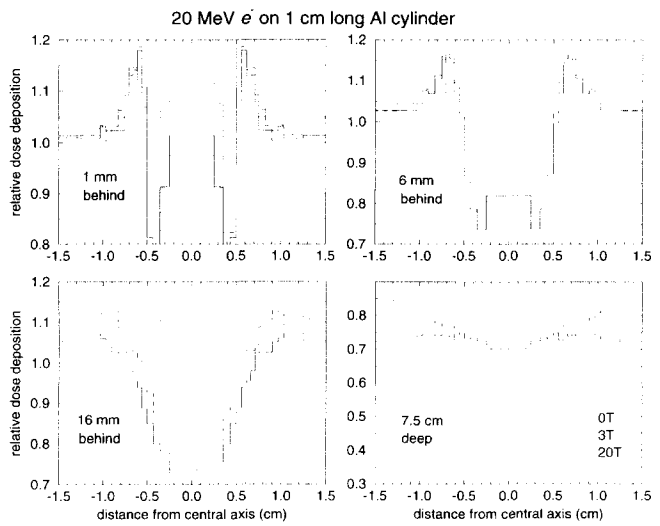

FIG. 12. The 20-MeV electrons are transported through water in the presence of uniform, longitudinal magnetic fields with strengths 0, 3, and 20 T. A 1-cm long, 1-cm radius aluminium inhomogeneity is placed at a depth of 2 mm in the phantom. Radial profiles of dose deposition are depicted 1, 6, and 16 mm behind the inhomogeneity, as well as at a 7.5-cm absolute depth.

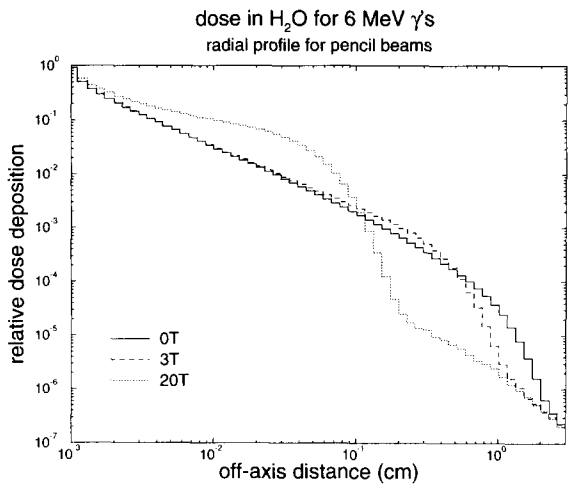

FIG. 13. A monoenergetic 6-MeV photon pencil beam is transported through water in the presence of uniform, longitudinal magnetic fields with strengths 0, 3, and 20 T. Radial dose deposition profiles are depicted.

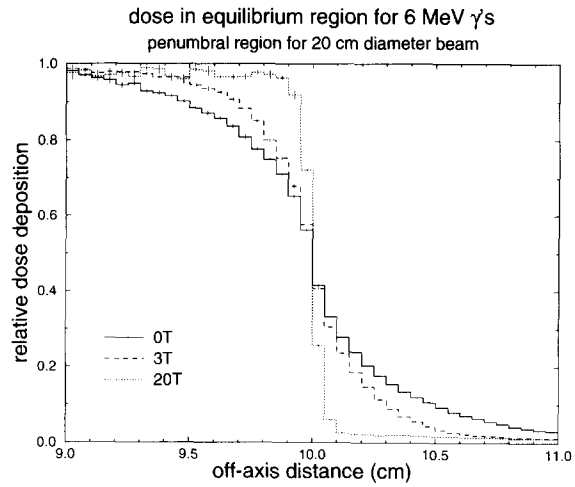

FIG. 14. A monoenergetic 6-MeV photon beam 10 cm in radius is transported through water in the presence of uniform, longitudinal magnetic fields with strengths 0, 3, and 20 T. Radial dose deposition profiles at equilibrium depth (3–6 cm in a 9-cm deep phantom) in the vicinity of the geometrical edge of the beam are depicted.

penumbra. The radial dose profile from a monoenergetic 6-MeV photon beam is shown in Fig. 13 for 0, 3, and 20 T. In this case, the phantom depth was 9 cm and the dose in the 3–6-cm portion was integrated and scored. This is the primary electron equilibrium region for this phantom, where the electrons set in motion by the primary electrons cannot escape. Evidence of confinement is seen for 0.5–2 cm for 3 T and 0.1–1 mm for 20 T. Again, the coincidence of the radial profiles at large radii indicates dose deposition from bremsstrahlung. However, this contribution is many orders of magnitude down from that near the vicinity of the beam.

B. Penumbra

The effect on the penumbra of broad beams is shown in Fig. 14 for a monoenergetic 6-MeV photon beam with 0-, 3-, and 20- T fields. Again, these results are taken from the 3–6-cm region in a 9-cm deep phantom. A substantial improvement for 3 T is observed while the 20-T results make the penumbra very sharp. The "wiggles" in the 20-T case are statistical in nature, despite 10^6 incident photons employed in the simulation. This is actually an artifact produced by the strong confinement of the electrons. Because of the strong lateral constraint, electron multiple scattering cannot smooth out any statistical irregularity present in the simulated input beam, and this is reflected in the shape of the 20-T curve, which is much more irregular than the 0- and 3-T cases.

It should be emphasised that the external magnetic field controls only the electron recoil contribution to the penumbra, and cannot have any influence on the other causes of penumbral shape—radiator spot size, smearing of the effective point source position due to electron diffusion through the radiator, radiator material, collimator placement and geometry, and the resultant photon energy spectrum. (The author is grateful to "Referee A" for pointing this out.) These factors may have to be controlled if the external magnetic field is to effect a noticeable improvement for photon therapies.

IV. CONCLUSIONS

In this work we investigated the effect of strong, longitudinal magnetic fields on dose deposition from electron and photon beams. It has been demonstrated that on the central axis of broad electron (and photon) beams, the dose deposited is independent of field strength. This means that for beams broad enough to establish lateral equilibrium on the central axis, dosimetry can be performed without the presence magnetic fields, which may have a deleterious effect on measurement instruments.

Clinical beams from machines that produce broad beams from scattering foils have point-source or quasi-point-source behavior. Although this upsets the equilibrium arguments presented above, it has been shown that the extra fluence of point-source beams can be exploited to produce sharper maxima. Consequently, dose may be deposited more advantageously and surface regions may be spared.

Penumbra in photon and electron beams can be controlled effectively by 3-T fields and practically eliminated by 20-T fields. The perturbative effects of small inhomogeneities on electron beam dose deposition can be greatly reduced by 20-T fields. At this field strength, electron beams become geometrical in character, much like proton fields. Consequently, flat energy deposition profiles can be produced at depth by the employment of a bolus applied at the surface to compensate for underlying heterogeneities.

These results beg the questions: Can the use of strong magnetic fields in electron beam therapy produce the advantages of proton beams but at lower cost? Can photon beam therapy benefit from magnetic fields as well? The answer to these questions depends largely on the cost of

producing strong, localized magnetic fields. Theoretically, the advantages are clear. There is one further advantage mentioned by Whitmire *et al.*[5]—the effective LET of δ rays may be greatly enhanced, since they will be "curled up" along the direction of the magnetic field lines. Therefore, there is not only the possibility controlling more advantageously the deposit of energy, but also the possibility that the energy deposited will be more effective for tumor control with magnetic fields than without them. However, there may be other biological effects symbiotic or otherwise with radiotherapy that may be associated with strong magnetic fields. Certainly, prudence is recommended before employing very strong fields under any circumstances.

ACKNOWLEDGMENTS

The author would like to thank Dr. J. Deasy and Dr. T. R. Mackie (University of Wisconsin, Madison) and Dr. M. Weinhous (Hahnemann University, Philadelphia) for their insights, M. Sharpe (London Regional Cancer Centre, Ontario) for his suggestion to investigate the effect of induced synchrotron radiation, and Dr. P. Andreo (Karolinska Institute, Stockholm), Dr. A. Nahum (Royal Marsden Hospital, London), and Dr. D. Rogers (National Research Council, Ottawa) for providing a critique of this manuscript.

APPENDIX: PROOF THAT THE CENTRAL-AXIS DEPTH DOSE IS INDEPENDENT OF MAGNETIC FIELD STRENGTH FOR BROAD, PARALLEL BEAMS

In this appendix a mathematical proof is given, demonstrating that the central axis depth-dose distribution from broad parallel electron beams incident normally on a flat phantom surface is unchanged by the presence of a uniform (spatially independent), longitudinal (direction parallel to the external beam) magnetic field. This has important implications for dosimetry and calibration, since instruments may be perturbed by magnetic fields in unpredictable ways.

The proof begins by a demonstration that constant, longitudinal magnetic fields do not change the electron fluence.

The equations of motion of a charged particle with charge e in a constant magnetic field in a vacuum[9] are

$$x_{\perp 1}=\frac{p^0_{\perp 2}}{eB}\left[1-\cos\left(\frac{eBx_{\parallel}}{p^0_{\parallel}}\right)\right]+\frac{p^0_{\perp 1}}{eB}\sin\left(\frac{eBx_{\parallel}}{p^0_{\parallel}}\right),$$
$$x_{\perp 2}=-\frac{p^0_{\perp 1}}{eB}\left[1-\cos\left(\frac{eBx_{\parallel}}{p^0_{\parallel}}\right)\right]+\frac{p^0_{\perp 2}}{eB}\sin\left(\frac{eBx_{\parallel}}{p^0_{\parallel}}\right). \quad (4)$$

In these equations, $B=|\mathbf{B}|$, and the direction of motion has been resolved into three components $(x_{\perp 1},x_{\perp 2},x_{\parallel})$, forming an orthogonal triad, with $x_{\parallel}$ aligned with the $\mathbf{B}$ field. The momentum is also resolved into the three components, $(p_{\perp 1},p_{\perp 2},p_{\parallel})$, with initial values, $(p^0_{\perp 1},p^0_{\perp 2},p^0_{\parallel})$ when $(x^0_{\perp 1},x^0_{\perp 2},x^0_{\parallel}) = (0,0,0)$. The component of momentum parallel to $\mathbf{B}$ is a constant of the motion, i.e., $p_{\parallel}=p^0_{\parallel}$, as is the energy and the velocity in the direction of the $\mathbf{B}$ field as well as the magnitude of the momentum in the direction perpendicular to the field.

The differential path length, ds, of the charged particle is given by

$$ds=\sqrt{(dx_{\perp 1})^2+(dx_{\perp 2})^2+(dx_{\parallel})^2}, \quad (5)$$

which may be shown to be

$$ds=\frac{|\mathbf{p}|}{p_{\parallel}}dx_{\parallel}. \quad (6)$$

Since $|\mathbf{p}|$ and $p_{\parallel}$ are constants, the path length between two planes at z_1 and z_2 is independent of the magnetic field strength, and is given by

$$s=\frac{|\mathbf{p}|}{p_{\parallel}}(z_2-z_1). \quad (7)$$

Therefore, in vacuum, the fluence in any planar region normal to the magnetic field is independent of the strength of the magnetic field.

To apply the argument to a uniform medium and broad incident beams, the transport of an electron may be considered to be a series of electron drifts interrupted by discrete interactions at $z_1,z_2,\ldots,z_n$. The magnetic field does not change the electron fluence between the points of interaction with the medium (by the above argument). Therefore, the electron fluence is a constant with depth, even in the presence of uniform media. For broad incident beams and semi-infinite media, the isotropy of the radial dimension cannot be broken by a uniform, longitudinal magnetic field. Since the only dimension over which physical quantities can change is in the depth dimension, and the fluence is not changed by the magnetic field, the dose deposited by broad beams is not altered by the strength of the longitudinal magnetic field.

For finite fields, as long as the beam is broad enough to establish lateral electron equilibrium in some region, the dose deposition in that region will be independent of the magnetic field strength. This applies in the example of Fig. 4.

[1]W. H. Bostick, "Possible techniques in direct-electron-beam tumor therapy," Phys. Rev. **77**, 564–565 (1950).
[2]M. S. Weinhous, R. Nath, and R. J. Schulz, "Enhancement of electron beam dose distributions by longitudinal magnetic fields: Monte Carlo simulations and magnet system optimization", Med. Phys. **12**, 598–603 (1985).
[3]M. Sempert, "New developments in high energy electron beam therapy with the 35 MeV Brown Boveri betatron," Radiology **74**, 105–107 (1960).
[4]C. C. Shih, "High energy electron radiotherapy in a magnetic field," Med. Phys. **2**, 9–13 (1975).
[5]D. P. Whitmire, D. L. Bernard, M. D. Peterson, and J. A. Purdy, "Magnetic enhancement of electron dose distribution in a phantom," Med. Phys. **4**, 127–131 (1977).
[6]R. Nath and R. J. Schulz, "Modification of electron-beam dose distributions by transverse magnetic fields," Med. Phys. **5**, 226–230 (1978).
[7]B. H. Paliwal, B. R. Thomadsen, and A. L. Wiley, "Magnetic modification of electron beam dose distributions," Acta Radiol. Oncol. **18**, 57–64 (1979).
[8]B. H. Paliwal, A. L. Wiley, B. W. Wessels, and M. C. Choi, "Magnetic field modification of electron-beam dose distributions in inhomogeneous media," Med. Phys. **5**, 404–408 (1978).

[9]A. F. Bielajew, "Electron transport in E and B fields," in *Monte Carlo Transport of Electrons and Photons*, edited by T. E. Jenkins, W. R. Nelson, A. Rindi, A. E. Nahum, and D. W. O. Rogers (Plenum, New York, 1987), pp. 421–434.

[10]W. R. Nelson, D. W. O. Rogers, and H. Hirayama, *The EGS4 Code System*, Stanford Linear Accelerator Report No. SLAC-265, Stanford, CA, 1985.

[11]A. F. Bielajew and D. W. O. Rogers, "PRESTA—the Parameter Reduced Electron-Step Transport Algorithm for electron Monte Carlo transport," Nucl. Instrum. Methods B **18**, 165–181 (1987).

[12]ICRU Report No. 37, *Stopping Powers for Electrons and Positrons*, ICRU, Washington DC, 1984.

[13]D. W. O. Rogers, S. Duane, and A. F. Bielajew, *Use of ICRU-37/NBS Collision Stopping Powers in the EGS4 System*, National Research Council of Canada Report No. PIRS-0173, 1989.

[14]S. Duane, D. W. O. Rogers, A. F. Bielajew, and W. R. Nelson, *Use of ICRU-37/NBS Radiative Stopping Powers in the EGS4 System*, National Research Council of Canada Report No. PIRS-0177, 1989.

[15]A. F. Bielajew and D. W. O. Rogers, "A comparison of experiment with Monte Carlo calculations of TLD response," Med. Phys. **13**, 609 (1986) (abstract).

[16]K. R. Shortt, C. K. Ross, A. F. Bielajew, and D. W. O. Rogers, "Electron beam dose distributions near small inhomogeneities," Phys. Med. Biol. **31**, 235–249 (1986).

[17]J. D. Jackson, *Classical Electrodynamics* (Wiley, New York, 1975), 2nd ed., p. 582.

[18]A. F. Bielajew and P. E. Wiebe, *EGS-Windows—A Graphical Interface to EGS*, National Research Council of Canada Report No. PIRS-0274, 1991.

[19]A. F. Bielajew and D. W. O. Rogers, "Differences in electron depth-dose curves calculated with EGS and ETRAN and improved energy-range relationships," Med. Phys. **13**, 687–694 (1986).

[20]A. F. Bielajew and D. W. O. Rogers, "Variance-reduction techniques," in *Monte Carlo Transport of Electrons and Photons*, edited by T. E. Jenkins, W. R. Nelson, A. Rindi, A. E. Nahum, and D. W. O. Rogers (Plenum, New York, 1987), pp. 407–420.

[21]J. Cygler, J. J. Battista, J. W. Scrimger, E. Mah, and J. Antolak, "Electron dose distributions in experimental phantoms: A comparison with 2D pencil beam calculations," Phys. Med. Biol. **32**, 1073–86 (1987).